

T2 Inverse techniques applied to the thermal characterization of shape-stabilized phase change materials

Jean-Luc Dauvergne* and Elena Palomo Del Barrio**

* Epsilon Fahrenheit, Esplanade des Arts et Métiers, F-33400 Talence, France, jldauvergne@epsilon-alcen.com

** Université de Bordeaux, I2M, UMR 5295, F-33400 Talence, France, elena.palomo-del-barrio@u-bordeaux1.fr

Abstract: A new experimental method for thermodynamic characterization of solid-liquid and shape-stabilized Phase Change Materials (PCM), through enthalpy-temperature function estimation, is described in this paper. The simplicity of the experimental setup is comparable to that of a hot plate and it allows fast and accurate characterization of large size samples. The heat transfer model corresponding to the experimental device is written as a constant parameters heat conduction model with a temperature dependent source term which contains all the information related to the phase change phenomenon. The enthalpy-temperature function is estimated by using an efficient inversion technique which only requires the measurement of the temperature at a point in the PCM. Through dimensionless and numerical tests, the capabilities and the limits of the proposed method have been investigated. A simple way to optimize the experimental conditions has been also proposed. An experimental test for characterization of a PCM composite is finally carried out to illustrate the appropriateness of those developments.

Keywords: PCM, enthalpy-temperature function, inverse method, experimental device

Nomenclature

Latin letters					
a	Thermal diffusivity	$m^2.s^{-1}$	G / PCM	Graphite foam/Phase Change Material composite	(-)
c	Specific heat at constant pressure	$J.kg^{-1}.k^{-1}$	IL	Insulated layer	(-)
f	Liquid fraction	(-)	k	Known	(-)
H	Volumetric enthalpy	$J.m^{-3}$	l	Liquid phase	(-)
H	Heaviside function	(-)	m	Measured	(-)
J	Cost function	K^2	PCM	Phase Change Material	(-)
k	Thermal conductivity	$W.m^{-1}.K^{-1}$	ref	Reference	(-)

L	Length, thickness	m	Superscript		
L_f	Latent heat	$J.kg^{-1}$	*	Dimensionless	(-)
n	Number of nodes	(-)	-	Mean	(-)
n_t	Number of time steps	(-)	.	Derivative	(-)
P_c	Dimensionless specific heat	(-)	T	Transpose	(-)
P_k	Dimensionless thermal conductivity	(-)	:	Estimated	(-)
q	Prescribed heat flux	$W.m^{-2}$	Greek letters		
Ste	Stefan number	(-)	α	Weighting function	(-)
t	Time variable	s	β	Weighting function	(-)
T	Temperature	K	K		
z	Space variable	m	θ	Dimensionless temperature	(-)
Subscripts			ΔT	Melting range	K
∞	Environment / infinite horizon	(-)	μ	Regularization parameter	(-)
0	Initial	(-)	ρ	Density	$kg.m^{-3}$
f	Melting	(-)	σ	Source	$K.s^{-1}$
s	Solid phase	(-)	τ	Dimensionless time variable	(-)
u	Unknown	(-)	φ	Dimensionless heat flux	(-)
			ψ	Dimensionless source term	(-)

2.1 Introduction

Phase Change Materials (PCM) could play an important role for an effective and economic use of thermal energy in the industrial sector (i.e. waste heat recovering, storage and reuse), as well as in power generation based on new conversion techniques (i.e. co-generation) and renewable energy resources (i.e. solar concentrating technologies). Moreover, PCM integration in lightweight buildings is expected to be a useful way to smooth indoor temperature variations and reduce overall heating or cooling demand.

Greatest asset of PCM is their capacity to store or release thermal energy over a narrow range of temperature, as well as latent heats ranging typically from 100 to 1000 kJ.kg^{-1} for PCM undergoing solid-liquid transformations. Recently, much work has been done on shape-stabilized PCM development. Such materials are generally made of an inert matrix (polymer, wood, concrete, graphite etc.) whose porosity is completely or partially filled with a solid-liquid phase change material. The inert matrix allows structural stability and retains the PCM when in liquid state. In addition, when made of a highly conductive material (i.e. graphite), it serves to enhance the PCM thermal conductivity.

Characterization of shape-stabilized PCM usually involves measurement of thermal conductivities and heat capacities of the solid and liquid phases, as well as transition temperatures and latent heat.

Some thermal properties can be estimated by quite standard methods. For instance, thermal conductivity and thermal diffusivity can be measured, respectively, by the hot plate method [1] and the flash method ([2], [3]). Dynamic hot probes methods allow simultaneous determination of thermal conductivity and capacity ([4]-[7]). As for specific heat and latent heat, specific DSC (Differential Scanning Calorimetric) tests are usually used ([8], [9]). Transition temperatures are better determined using DTA (Differential Thermal Analysis) methods.

The estimation of the enthalpy-temperature function is more difficult. It can be obtained using DSC in isothermal step mode ([10], [11]) but such tests generally require very small samples (some few millilitres), so that they become inappropriate for testing heterogeneous materials with large-size representative volumes. This problem could be partially overcome using the T-History method ([12], [13]), a cheap and easy way for the determination of latent heats and specific heats. Unfortunately, T-History method is unable to provide reliable estimations of transition temperatures and enthalpy-temperature functions ([14], [15]). Another problem is the very long testing times (from one day to one week) required to obtain the enthalpy-temperature function by DSC.

To overcome such problems, an experimental method for complete characterization (thermal properties and enthalpy-temperature function) of PCM has been developed recently ([16]-[18]). The simplicity of the proposed experimental device is comparable to that of T-History method: a cylinder of PCM which is heated/cooled in a furnace following specific temperature patterns (steps, isotherms and ramps) and temperature measurements at one-single point within the PCM. The enthalpy-temperature function is retrieved by inversion of an appropriate heat transfer model instead of by simple energy balance techniques. It has been proven that, contrary to the T-History method, the proposed method allows unbiased estimations of the enthalpy-temperature functions. However, the method is intrusive and the testing time required remains significant (one day) even if shorter than in “isothermal step mode” DSC tests.

In this paper, we propose a non-intrusive method for complete thermal characterization of PCM based on a smaller and simpler experimental device. The objective is to be able to estimate the enthalpy-temperature function of a PCM (including highly heterogeneous PCMs) in few minutes. This function is retrieved by solving a problem of time-dependent sources estimation by inversion of a linear heat conduction model. In this paper it will be shown that those sources are the output of a linear and invariant state model whose inputs are the measured temperatures. Enthalpy-temperature function is thus calculated by a simple time integration.

The paper describes i) the proposed setup and the experimental protocol, ii) the associated heat transfer model and iii) the inverse method mentioned above. It also includes a numerical study that shows the

capabilities and the limits of the experimental method proposed and provides recommendations to design the setup. Finally, an experimental test for characterization of a graphite foam/PCM composite is carried out to illustrate the appropriateness of our developments.

2.2 Experimental setup and heat transfer modelling

This section includes a description of the experimental device and the experimental protocol and it establishes modelling assumptions and governing equations. The thermal behaviour of the shape-stabilized PCM during melting-solidification is described as a constant-parameters heat conduction problem with a temperature dependent source term which contains all information related to the phase change phenomenon.

2.2.1 Experimental setup

The proposed experimental device looks like hot plate setups usually used for thermal conductivity measurement (see [19] and [20] for example). It is a layered structure in which the sample of the PCM to be tested is sandwiched between a heating element and an insulation layer with known thermal properties. From the bottom to the top, it comprises (see Fig. 1): a) a Peltier element to heat/cool the sample; b) the PCM sample with known thickness (L_{PCM}); and c) an insulation layer of thickness L_{IL} and whose thermal properties is known. A thin flat sensor for heat flux measurements is placed at the interface between the Peltier element and the sample. A temperature sensor (thermocouple type K) is placed between the sample and the insulation layer in order to measure the thermal response of the PCM at its top face (T_m). A second thermocouple (type K) is placed at the top of the insulation layer to measure the temperature at this boundary (T_∞).

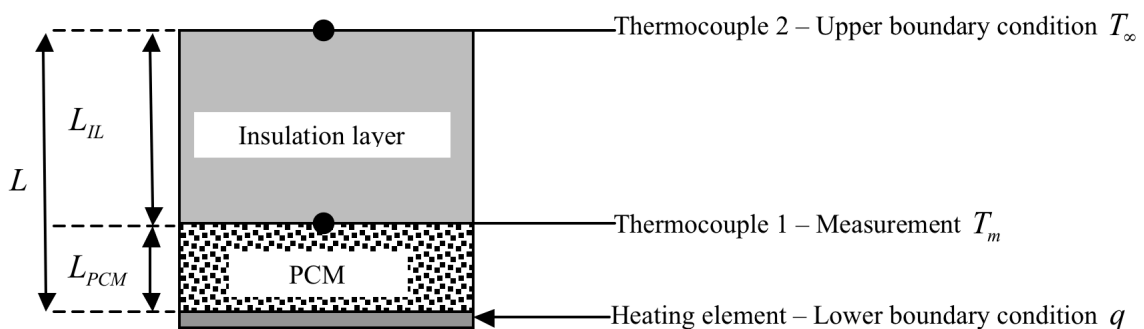


Figure 1: Scheme of the experimental setup

2.2.2 Experimental protocol

As sketched in Figure, three main periods can be distinguished in the experiments:

- a- *Start-up period* (from times $t = t_0 = 0$ to $t = t_1$), where the device is at uniform temperature in thermal equilibrium with its environment ($T_1 = T_\infty$) and the Peltier element is off.

- b- *Melting period* (from $t = t_1$ to $t = t_3$), where a uniform and constant heat flux (q_{\max}) is applied on the bottom face of the sample. The temperature T_m at the top side of the sample increases up to a temperature T_3 above the melting temperature T_f .
- c- *Solidification period* (from $t = t_3$ to $t = t_4$), where the heat flux is reversed ($q = -q_{\max}$) and T_m decreases from T_3 to a temperature T_4 close to T_∞ to observe the thermal behaviour of the studied material during solidification.

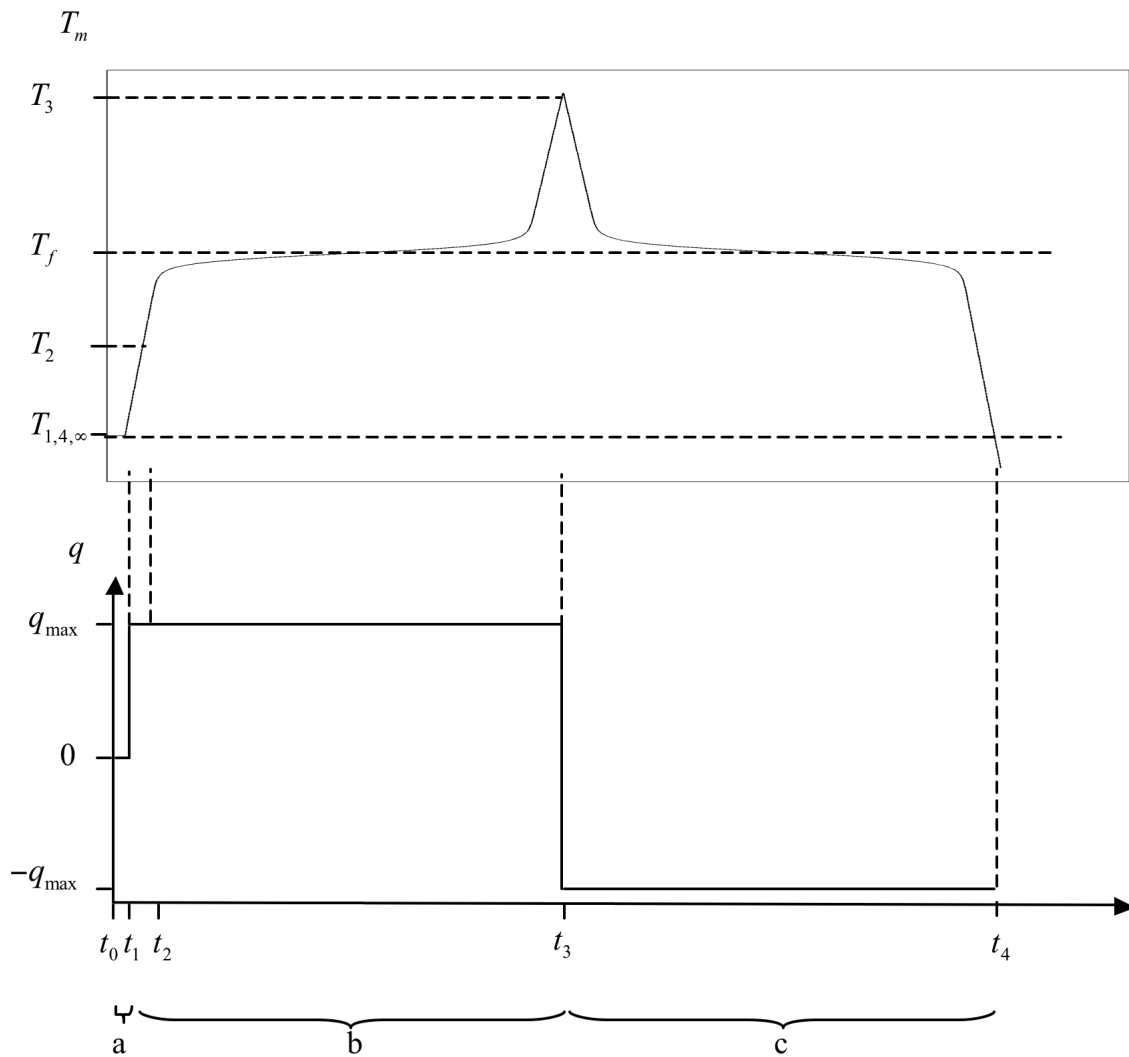


Figure 2: Sketch of the experimental protocol and corresponding measured temperature T_m

Throughout the experiment, the collected data are: the heat flux applied at the bottom face of the sample, $q(t)$, the temperature at the top face of the sample, $T_m(t)$, and the temperature at the top of the insulation layer, $T_\infty(t)$. As discussed later, data recorded from t_1 to t_2 before the melting of the sample ($T < T_f$), can

be used to estimate the thermal conductivity and the thermal capacity of the PCM in solid state [21]. On the contrary, the estimation of the enthalpy function is carried out using all data recorded from t_0 to t_4 .

2.2.3 Modelling assumptions

Basic assumptions employed for shape-stabilized PCM melting/solidification modelling, valid across a significant number of systems, are:

- a) The PCM can be seen as a continuous medium at the macroscopic scale. The volume averaging method has been recently used [18] to derive macroscopic energy equations within PCM infiltrated matrices. Formal relationships between effective macroscopic and local properties and functions (i.e. enthalpy-temperature function) have been established. It's also assumed as an isotropic material.
- b) Convective heat exchanges within the PCM are negligible. One notices that porosity of shape-stabilized PCM is usually controlled to prevent PCM leakage when in liquid state.
- c) The thermal properties (heat capacity and thermal conductivity) of the PCM are constant within each phase but heat capacity could be discontinuous between the solid and liquid. On the contrary, thermal conductivity is assumed to be independent of the PCM state.
- d) Phase change occurs at constant pressure. It can take place at a single temperature and constant composition (i.e. pure substances, eutectic mixtures...) or over a range of temperatures (i.e. alloys, impure materials...). In the first case, a sharp melting/solidification front separates liquid and solid phases within the domain; while in the second case, a two-phase zone ("mushy region") appears between the solid and liquid sub-domains.
- e) Under-cooling is negligible, or at least of non-random nature. This is generally true for organic PCM (i.e., paraffin, fatty acids, esters etc.). For inorganic PCM (i.e. salts) significant under-cooling can be observed. However, it is often reduced (or at least stabilized) using nucleation agents.
- f) For multi-component phase change materials undergoing transformation over a range of temperatures, no segregation during solidification is also assumed. This means that the density of the solid phase is closed to that of the liquid phase.

Moreover, the form factor (height/width) of the device is small enough so that one dimensional heat transfer can be assumed.

(1) Energy equations

According to the previous hypothesis, energy conservation equation in a one dimensional case can be written as:

$$\frac{\partial H(z,t)}{\partial t} = k(z) \frac{\partial^2 T(z,t)}{\partial z^2} \quad \forall z \in (0,L), \forall t > 0 \quad (2.1)$$

Where $H(z,t)$ and $T(z,t)$ are respectively the volumetric enthalpy and the temperature of the system at z and at time t . k is the thermal conductivity at the point z .

The relation linking the enthalpy and the temperature is:

$$H = [(1-f)\rho c_s + f\rho c_l]T + \rho L_f f \quad (2.2)$$

Where ρ , c_x and L_f represent the density, the specific heat in liquid ($x=l$) or solid ($x=s$) state and the latent heat of the PCM. On the other hand, f is the liquid fraction. For PCM undergoing melting/solidification at a single temperature, the liquid fraction is given by $f = H(T - T_f)$, where H represents the Heaviside function and T_f is the phase change (melting or solidification) temperature. For melting/solidification taking place over a range of temperatures, differential scanning calorimetric

measurements are usually required to determine the relationship existing between the liquid fraction and the temperature. In order to simulate all kind of behaviours, a model of liquid fraction can also be used. We can consider for example:

$$f = \frac{1}{2} \left[1 - \tanh \left(\frac{T_f - T}{\Delta T} \right) \right] \quad (2.3)$$

where ΔT is the range of temperature where the phase change occurred ($\Delta T = T_{liquidus} - T_{solidus}$). We note that for $T < T_{solidus}$, $f \approx 0$; while for $T > T_{liquidus}$, $f \approx 1$. The interval $[T_{solidus}, T_{liquidus}]$ defines the « mushy region » with the coexistence of the liquid and solid state ($0 < f < 1$). In addition, the equation (2.3) allows the simulation of the two distinct behaviours: for $\Delta T \rightarrow 0$ the transformation is close to a monovariant one and $\Delta T > 0$ emulate a transformation over an interval of temperature. Concerning the insulated layer, there is no phase change phenomenon: $\forall T$, $f = 0$. and equation (2.2) becomes $H = \rho c_s T = \rho c_{IL} T$, where ρc_{IL} represents the specific heat of the layer.

Using the equation (2.2), equation (2.1) becomes:

$$\frac{\partial T(z,t)}{\partial t} = \frac{k(z)}{\rho c_s(z)} \frac{\partial^2 T(z,t)}{\partial z^2} + \sigma(z,t;T) \quad \forall z \in (0,L), \forall t > 0 \quad (2.4)$$

with

$$\sigma(z,t;T) = \frac{1}{\rho c_s} \frac{\partial (\Delta \rho c T(z,t) + \rho L_f)}{\partial t} f(z,t;T) \quad (2.5)$$

and $\Delta \rho c = \rho c_l - \rho c_s$. Equation (2.4) is written like a constant parameters heat conduction problem with a temperature dependent source term $\sigma(z,t;T)$ that contains all information related to the phase change phenomenon. We notice that $\sigma(z,t;T) = 0$ for the insulated layer and for the PCM in solid or liquid phase. We also observe that the knowledge of the source term $\sigma(z,t;T)$ allows obtaining the enthalpy-temperature function of the PCM. As:

$$\frac{\partial H(z,t)}{\partial t} = \rho c_s \left[\frac{\partial T(z,t)}{\partial t} - \sigma(z,t;T) \right] \quad (2.6)$$

We obtain, by a simple time integration:

$$H(z,t) - H(z,0) = \rho c_s \left[(T(z,t) - T(z,0)) - \int_{\tau=0}^t \sigma(z,\tau;T) d\tau \right] \quad (2.7)$$

The continuity equation at the interface between the PCM and the insulated layer is written:

$$-k_{PCM} \frac{\partial T(z,t)}{\partial z} \Big|_{z=L_{PCM}} = -k_{IL} \frac{\partial T(z,t)}{\partial z} \Big|_{z=L_{PCM}} \quad \forall t > 0 \quad (2.8)$$

where k_{PCM} and k_{IL} represent the thermal conductivities of the phase change material and the insulated layers, respectively.

According to the experimental device, the upper Dirichlet boundary condition is:

$$T(z, t) \Big|_{z=L} = T_{\infty}(t) \quad \forall t > 0 \quad (2.9)$$

where $T_{\infty}(t)$ represents the prescribed temperature, controlled by the thermocouple 2 (See Figure 1). The lower side of the PCM is submitted to a prescribed heat flux, denoted q , generated by a heating element:

$$-k_{PCM} \frac{\partial T(z, t)}{\partial z} \Big|_{z=0} = q(t) \quad \forall t > 0 \quad (2.10)$$

As for initial conditions, we assume: $T(z, t = 0) = T_{\infty}, \forall z \in (0, L)$.

(2) State-space model

Since no general theory is currently available for the analytic solution of partial differential equations, approximate numerical solutions are the only practical alternative to which scientists engineers usually resort in order to solve this type of equations. The spatial discretization (finite volume method in this paper) of equations (2.1) and (2.8)-(2.10) leads to a finite dimensional formulation of the general form:

$$\frac{d\mathbf{H}(t)}{dt} = \mathbf{A}\mathbf{T}(t) + \mathbf{B}\mathbf{U}(t) \quad (2.11)$$

For each time step, \mathbf{H} ($n \times 1$) is the vector of enthalpies at the n nodes of discretization grid. Matrix \mathbf{A} ($n \times n$) describes heat exchanges among the finite volumes within the multilayer and matrix \mathbf{B} ($n \times 2$) ensures the thermal connection between the device and its environment: \mathbf{U} (2×1) is the vector of the boundary conditions (prescribed temperature and heat flux). Both \mathbf{A} and \mathbf{B} are constant matrices whose elements depend of thermal conductivities and space steps values (PCM and insulated layer). The conversion of the enthalpy to the temperature, or temperature to enthalpy, is done using equations (2.2) and (2.3). The measured temperature at the interface between the PCM and the insulated layer can be written: $\mathbf{T}_m(t) = \mathbf{J}\mathbf{T}(t)$, where \mathbf{J} is the ($2 \times n$) appropriate matrix of zeros and scalars dependent on the thermal conductivity of each layer. For a numerical study purpose, the results obtained by this state-space are considered in the following as the exact ones.

Concerning the enthalpy-temperature function estimation, the used model is:

$$\frac{d\mathbf{T}(t)}{dt} = \mathbf{C}^{-1}\mathbf{A}\mathbf{T}(t) + \mathbf{C}^{-1}\mathbf{B}\mathbf{U}(t) + \boldsymbol{\sigma}(t; T) \quad (2.12)$$

\mathbf{T} ($n \times 1$) is the vector of temperatures at the n nodes of discretization grid and $\boldsymbol{\sigma}$ ($n \times 1$) is the vector of sources. Matrix \mathbf{C} ($n \times n$) contains the specific heat of the PCM in solid phase and the one of the insulated layer. As previously, the measured temperature field \mathbf{T}_m is given by $\mathbf{T}_m(t) = \mathbf{J}\mathbf{T}(t)$.

2.3 Inverse method for PCM characterization

In this section is presented the inversion method for thermodynamic characterization of a shape-stabilized PCM from a one-single experiment and a one-single measurement point of temperature. The thermal properties of the insulated layer as the boundary conditions, i.e. the heat flux and the temperature of the environment for the Dirichlet condition on the upper side of the device, are assumed well known. The thermal properties of the PCM, k_{PCM} and $\rho c_{s,PCM}$, are assumed as known or estimated by a classical way (see the previous section).

2.3.1 Enthalpy-temperature functions estimation

The enthalpy-temperature function is estimated from the measured temperature field $T_m(t)$ at the interface between the PCM and the insulated layer. It's assumed that the solicitations $U(t)$ ($T_\infty(t)$ and $q(t)$) as well as thermal parameters (ρc_s and k) of both layers, are well-known or estimated using the first part of the experimental protocol. The unknowns of the problem are the thermal fields $T(z,t)$ within each layer of the device and the source terms $\sigma(z,t;T)$. If we are able to estimate $T(z,t)$ and $\sigma(z,t;T)$, equation (2.7) leads to the enthalpy-temperature we are looking for. Hence, let us consider the problem of estimating the thermal field $T(z,t)$ and the source term $\sigma(z,t;T)$ in equation (2.4) from the measured data $T_m(t)$ and the known boundary conditions $U(t)$. This is an ill-posed inverse problem in the sense of Hadamard [22], because the solution may be not unique or not continuous with respect to the given data. To overcome such a difficulty a large variety of techniques have been proposed ([23]-[27]). Tikhonov, Alifanov, and others from the Russian school proposed to cast the ill-posed inverse problem into an optimisation problem with a regularised objective function. Hence, the problem we have can be mathematically formulated as a problem of finding $\sigma(z,t;T)$ that minimises the quadratic criterion:

$$\mathcal{J} = \frac{1}{2} \int_{t=0}^{t_{end}} \alpha [\tilde{T}_m(t; \tilde{\sigma}) - T_m(t)]^2 dt + \frac{\mu}{2} \int_{t=0}^{t_{end}} \beta \tilde{\sigma}^2(M, t; T) dt \quad (2.13)$$

where $\mu > 0$ is a Tikhonov regularization parameter [27], α and β are continuous weighting functions. After spatial discretization (n nodes), equation (2.13) becomes:

$$\mathcal{J} = \frac{1}{2} \int_{t=0}^{t_{end}} [J\tilde{T}(t; \tilde{\sigma}) - T_m(t)]^T Q [J\tilde{T}(t; \tilde{\sigma}) - T_m(t)] dt + \frac{\mu}{2} \int_{t=0}^{t_{end}} \tilde{\sigma}^T(t) R \tilde{\sigma}(t) dt \quad (2.14)$$

where Q (2×2) and R ($n \times n$) are positive definite matrices. They come from the discretization of the weighting functions α and β . $\tilde{\sigma}(t)$ ($n \times 1$) is the discrete version of the unknown source term field, also used to calculate the temperature field $\tilde{T}(t; \tilde{\sigma})$ ($n \times 1$) through model (2.12).

Taking into account the linear nature of equations (2.4), (2.9) and (2.10), superposition principle allows writing:

$$T(t; \sigma) = T_k(t) + T_u(t; \sigma) \quad (2.15)$$

The known part $\mathbf{T}_k(t)$ of the thermal field $\mathbf{T}(t; \boldsymbol{\sigma})$ is the system response to the boundary conditions $\mathbf{U}(t)$ and the unknown part $\mathbf{T}_u(t; \boldsymbol{\sigma})$ represents its response to $\boldsymbol{\sigma}(t)$. In the same way and with similar subscripts, we can write $\mathbf{JT}(t; \boldsymbol{\sigma}) = \mathbf{JT}_k(t) + \mathbf{JT}_u(t; \boldsymbol{\sigma})$ and $\mathbf{T}_m(t) = \mathbf{T}_{m,k}(t) + \mathbf{T}_{m,u}(t)$.

Thus, the cost function J can be written:

$$\mathcal{J} = \frac{1}{2} \int_{t=0}^{t_{end}} [\mathbf{JT}_u(t; \tilde{\boldsymbol{\sigma}}) - \mathbf{T}_{m,u}(t)]^T \mathbf{Q} [\mathbf{JT}_u(t; \tilde{\boldsymbol{\sigma}}) - \mathbf{T}_{m,u}(t)] dt + \frac{\mu}{2} \int_{t=0}^{t_{end}} \tilde{\boldsymbol{\sigma}}^T(t) \mathbf{R} \tilde{\boldsymbol{\sigma}}(t) dt \quad (2.16)$$

where $\mathbf{T}_{m,u}(t)$ is the unknown part of the observations $\mathbf{T}_m(t)$ and $\mathbf{JT}_u(t; \tilde{\boldsymbol{\sigma}})$ is the unknown part of the estimated observation field $\tilde{\mathbf{T}}(t; \tilde{\boldsymbol{\sigma}})$.

Applying Lagrange's theory and calculus of variation rules, it can be show that the minimum of the cost function J is achieved for the solution $\tilde{\boldsymbol{\sigma}}(t)$ of the three following problems [28]:

a) *Direct problem*

$$\dot{\tilde{\mathbf{T}}}_u(t; \tilde{\boldsymbol{\sigma}}) = \mathbf{A} \tilde{\mathbf{T}}_u(t; \tilde{\boldsymbol{\sigma}}) + \mathbf{B} \tilde{\boldsymbol{\sigma}}(t) \quad (2.17)$$

\mathbf{A} is the matrix ($n \times n$) describing the conductive transfers within the system and \mathbf{B} is the matrix ($n \times n$) describing coupling of the system with the source term.

b) *Adjoint problem*

$$-\dot{\boldsymbol{\lambda}}(t) = \mathbf{A}^T \boldsymbol{\lambda}(t) + \mathbf{J}^T \mathbf{Q} \mathbf{J} \tilde{\mathbf{T}}_u(t; \tilde{\boldsymbol{\sigma}}) - \mathbf{J}^T \mathbf{Q} \mathbf{T}_{m,u}(t) \quad (2.18)$$

$\boldsymbol{\lambda}(t)$ is the co-state vector of $\tilde{\mathbf{T}}_u(t; \tilde{\boldsymbol{\sigma}})$.

c) *Stationarity condition*

$$\tilde{\boldsymbol{\sigma}}(t) = -\mathbf{R}^{-1} \mathbf{B}^T \boldsymbol{\lambda}(t) \quad (2.19)$$

Introducing the stationarity condition (2.19) into the direct problem (2.17), we obtain the system of ordinary differential equations given by:

$$\begin{cases} \dot{\tilde{\mathbf{T}}}_u(t; \tilde{\boldsymbol{\sigma}}) = \mathbf{A} \tilde{\mathbf{T}}_u(t; \tilde{\boldsymbol{\sigma}}) - \mathbf{B} \mathbf{R}^{-1} \mathbf{B}^T \boldsymbol{\lambda}(t) \\ -\dot{\boldsymbol{\lambda}}(t) = \mathbf{A}^T \boldsymbol{\lambda}(t) + \mathbf{J}^T \mathbf{Q} \mathbf{J} \tilde{\mathbf{T}}_u(t; \tilde{\boldsymbol{\sigma}}) - \mathbf{J}^T \mathbf{Q} \mathbf{T}_{m,u}(t) \end{cases} \quad (2.20)$$

This system can be easily solved using the "sweep method" ([28], [29]) which assumes that $\tilde{\mathbf{T}}_u(t; \tilde{\boldsymbol{\sigma}})$ and $\boldsymbol{\lambda}(t)$ satisfy relation like:

$$\boldsymbol{\lambda}(t) = \mathbf{S}(t) \tilde{\mathbf{T}}_u(t; \tilde{\boldsymbol{\sigma}}) + \mathbf{v}(t) \quad (2.21)$$

for an unknown matrix function $\mathbf{S}(t)$ and vector function $\mathbf{v}(t)$. The solution of the inverse problem is the given by:

$$\tilde{\sigma}(t) = -\mathbf{K}(t)\tilde{\mathbf{T}}_u(t; \tilde{\sigma}) - \mathbf{R}^{-1}\mathbf{B}^T\mathbf{v}(t) \quad (2.22)$$

with

$$\begin{cases} \dot{\tilde{\mathbf{T}}}_u(t; \tilde{\sigma}) = [\mathbf{A} - \mathbf{BK}(t)]\tilde{\mathbf{T}}_u(t; \tilde{\sigma}) - \mathbf{BR}^{-1}\mathbf{B}^T\mathbf{v}(t) \\ -\dot{\mathbf{v}}(t) = [\mathbf{A} - \mathbf{BK}(t)]^T\mathbf{v}(t) - \mathbf{J}^T\mathbf{Q}\mathbf{T}_{m,u}(t) \end{cases} \quad (2.23)$$

and $\tilde{\mathbf{T}}_u(0) = \mathbf{T}_0$ and $\mathbf{v}(t_f) = 0$. The time-varying matrix $\mathbf{K}(t)$ is called Kalman gain. It is given by:

$$\mathbf{K}(t) = \mathbf{R}^{-1}\mathbf{B}^T\mathbf{S}(t) \quad (2.24)$$

where $\mathbf{S}(t)$ is the unique solution of the Riccati equation:

$$-\dot{\mathbf{S}}(t) = \mathbf{A}^T\mathbf{S}(t) + \mathbf{S}(t)\mathbf{A} - \mathbf{S}(t)\mathbf{B}\mathbf{R}^{-1}\mathbf{B}^T\mathbf{S}(t) + \mathbf{J}^T\mathbf{Q}\mathbf{J} \quad (2.25)$$

For a long enough time interval $[0, t_{end}]$ (infinite horizon problem), the solution of the Riccati equation above converges to a limiting solution \mathbf{S}_∞ :

$$\mathbf{0} = \mathbf{A}^T\mathbf{S}_\infty + \mathbf{S}_\infty\mathbf{A} - \mathbf{S}_\infty\mathbf{B}\mathbf{R}^{-1}\mathbf{B}^T\mathbf{S}_\infty + \mathbf{J}^T\mathbf{Q}\mathbf{J} \quad (2.26)$$

The system (2.23) become :

$$\begin{cases} \begin{bmatrix} \dot{\tilde{\mathbf{T}}}_u(t; \tilde{\sigma}) \\ -\dot{\mathbf{v}}(t) \end{bmatrix} = \begin{bmatrix} (\mathbf{A} - \mathbf{BK}_\infty) & -\mathbf{BR}^{-1}\mathbf{B}^T \\ \mathbf{0} & (\mathbf{A} - \mathbf{BK}_\infty)^T \end{bmatrix} \begin{bmatrix} \tilde{\mathbf{T}}_u(t; \tilde{\sigma}) \\ \mathbf{v}(t) \end{bmatrix} + \begin{bmatrix} \mathbf{0} \\ \mathbf{J}^T\mathbf{Q} \end{bmatrix} \mathbf{T}_{m,u}(t) \\ \tilde{\sigma}(t) = \begin{bmatrix} -\mathbf{K}_\infty & -\mathbf{R}^{-1}\mathbf{B}^T \end{bmatrix} \begin{bmatrix} \tilde{\mathbf{T}}_u(t; \tilde{\sigma}) \\ \mathbf{v}(t) \end{bmatrix} \end{cases} \quad (2.27)$$

with $\mathbf{K}_\infty = \mathbf{R}^{-1}\mathbf{B}^T\mathbf{S}_\infty$. The solution of the inverse problem is simply obtained by time integration of a state model where solicitations are the measurements.

Step-by-step, the inverse problem solving involves:

1. Calculation of the time-invariant matrices \mathbf{S}_∞ and \mathbf{K}_∞ . We note that they are independent on the system state trajectory, so they can be calculated off-line.
2. Calculation of $\mathbf{v}(t)$ by time-integration of the equation $-\dot{\mathbf{v}}(t) = [\mathbf{A} - \mathbf{BK}(t)]^T\mathbf{v}(t) - \mathbf{J}^T\mathbf{Q}\mathbf{T}_{m,u}(t)$, with $\mathbf{v}(t_{end}) = 0$. We note that the time is measured backwards from the final time t_{end} to the initial time $t_0 = 0$. However, by defining a new time variable $\tau = t_{end} - t$, the corresponding τ domain becomes from $\tau = 0$ to t_{end} .

3. Calculation of $\tilde{\mathbf{T}}_u(t; \tilde{\boldsymbol{\sigma}})$ by time-integration of the equation $\dot{\tilde{\mathbf{T}}}_u(t; \tilde{\boldsymbol{\sigma}}) = [\mathbf{A} - \mathbf{BK}_\infty(t)]\tilde{\mathbf{T}}_u(t; \tilde{\boldsymbol{\sigma}}) - \mathbf{BR}^{-1}\mathbf{B}^T\mathbf{v}(t)$, with $\mathbf{T}_u(0) = \mathbf{T}_0$.
4. Calculation of the unknown field: $\tilde{\boldsymbol{\sigma}}(t) = -\mathbf{K}_\infty\tilde{\mathbf{T}}_u(t; \tilde{\boldsymbol{\sigma}}) - \mathbf{R}^{-1}\mathbf{B}^T\mathbf{v}(t)$.

Solving this inverse problem allows the estimation of the source term $\boldsymbol{\sigma}(t)$ in every time step and in every node of discretization.

Knowing $\tilde{\mathbf{T}}(t; \tilde{\boldsymbol{\sigma}}) = \mathbf{T}_k(t) + \tilde{\mathbf{T}}_u(t; \tilde{\boldsymbol{\sigma}})$, $\tilde{\mathbf{T}}_u(t; \tilde{\boldsymbol{\sigma}})$ was calculated in above step 3), and $\tilde{\boldsymbol{\sigma}}(t)$ (step 4), it's possible to calculate the enthalpy-temperature function $\tilde{\mathbf{H}}(t; \tilde{\boldsymbol{\sigma}})$ we want to determine:

$$\tilde{\mathbf{H}}(t; \tilde{\boldsymbol{\sigma}}) = \rho c_s \left(\tilde{\mathbf{T}}(t; \tilde{\boldsymbol{\sigma}}) + \int_{t=0}^{t_f} \tilde{\boldsymbol{\sigma}}(t) d\tau \right) \quad (2.28)$$

The enthalpy-temperature function, like the source term, is estimated for all time steps and nodes of discretization. We can also notice that its possible to estimate $\boldsymbol{\sigma}(t)$ only for the nodes of discretization within the PCM, indeed, $\boldsymbol{\sigma}(t) = \mathbf{0}$ at the nodes corresponding to the insulated layer:

$$\tilde{\mathbf{H}}_{PCM}(t; \tilde{\boldsymbol{\sigma}}_{PCM}) = \rho c_{s,PCM} \left(\tilde{\mathbf{T}}_{PCM}(t; \tilde{\boldsymbol{\sigma}}_{PCM}) + \int_{t=0}^{t_f} \tilde{\boldsymbol{\sigma}}_{PCM}(t) d\tau \right) \quad (2.29)$$

Thus, $\tilde{\mathbf{H}}_{PCM}(t; \tilde{\boldsymbol{\sigma}}_{PCM})$ is a $(n_{PCM} \times n_t)$ matrix with n_{PCM} the number of nodes of discretization of the PCM layer and n_t the number of time steps. The representation of $\tilde{\mathbf{H}}_{PCM}(t; \tilde{\boldsymbol{\sigma}}_{PCM})$ against the corresponding elements of $\tilde{\mathbf{T}}_{PCM}(t; \tilde{\boldsymbol{\sigma}}_{PCM})$ leads to n_{PCM} enthalpy-temperature functions. In order to obtain only one enthalpy-temperature function, representative of the studied PCM, we calculate the mean $\bar{\mathbf{H}}_{PCM}(\tilde{\mathbf{T}}_{PCM})$ of those n_{PCM} estimated functions in each elements of $\tilde{\mathbf{T}}_{PCM}(t; \tilde{\boldsymbol{\sigma}}_{PCM})$. One notices that the choice of n_{PCM} for enthalpy-temperature estimation is independent of the n_{PCM} devoted to the simulation of the thermal fields (Eq. (2.11)). In this work, $n_{PCM} = 2$ for enthalpy-temperature function estimation and $n_{PCM} = 20$ for the simulation.

Concerning the Tikhonov regularization parameter μ , it must be chosen carefully: a too low value or a too high one leads to a bad estimation of the enthalpy-temperature function. A very convenient tool to chose this parameter is the ‘‘L-curve’’ representation [30]. Thus, the Frobenius norm $\|\tilde{\mathbf{T}}_m(t; \tilde{\boldsymbol{\sigma}}, \mu) - \mathbf{T}_m(t)\|$ is plotted for different values of μ against the norm of the estimated source term field $\tilde{\boldsymbol{\sigma}}(t)$. \mathbf{T}_m is the measurement and $\tilde{\mathbf{T}}_m(t; \tilde{\boldsymbol{\sigma}}, \mu)$ is calculated, trough the model (2.12), using the estimated $\tilde{\boldsymbol{\sigma}}(t)$ for a given μ . The best value of the regularization parameter is thus directly obtained at the minimum of the L-curve (Figure-a).

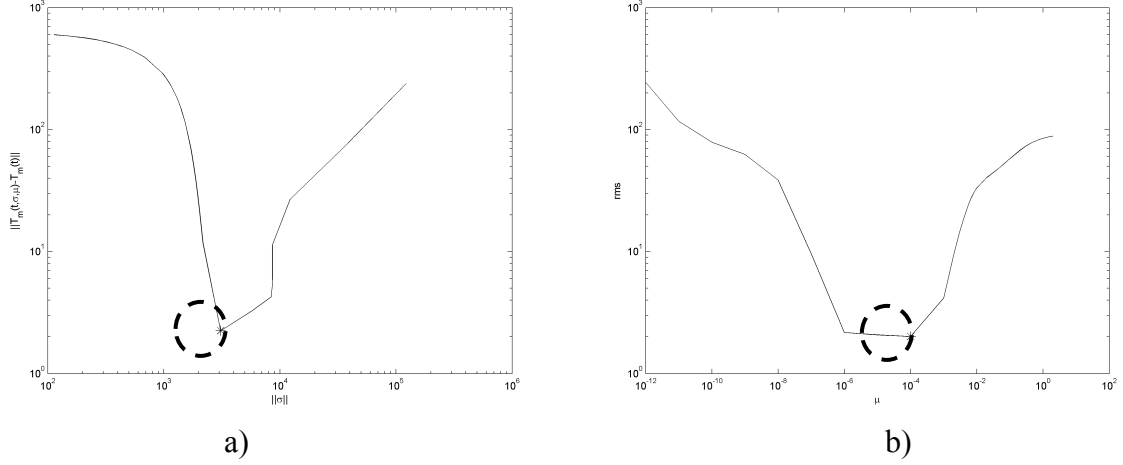


Figure 3: a) Representation of a L-curve b) rms of the enthalpy-temperature function for different regularization parameters. Dashed circle: localization of the best regularisation parameter

The proposed estimation is very fast and a large range of regularization parameters can be tested without significant loss of calculation time. In this paper, 15 different values of μ covering a range from 1.10^{-12} to 1 are examined.

The quality of the estimated enthalpy-temperature function $\bar{H}_{PCM}(t; \tilde{\sigma}_{PCM})$ is evaluated as:

$$rms = \sqrt{\frac{1}{n_t} \sum_{i=1}^{n_t} (\bar{H}_{PCM}(\tilde{T}_{PCM}) - H_{PCM}(T_{PCM}))^2} \quad (2.30)$$

where $H_{PCM}(T_{PCM})$ represents the true enthalpy-temperature function (calculated using equations (2.2) and (2.3)). We observe (Figure-b) that the rms is minimum for the value of μ obtained using the L-curve. Thus, the L-curve provides a powerful tool for an easy and accurate estimation of the enthalpy-temperature function.

2.4 Numerical design of the device

In this section, the dimensionless form of the previous problem is studied in order to establish some limits of the proposed experimental device and to provide recommendations to design it. After a presentation of the dimensionless model, a large range of configurations is simulated through different sets of dimensionless parameters.

2.4.1 Dimensionless problem

Some change of variables are applied in the problem described in the previous section:

$$\begin{aligned} \theta &= \frac{T - T_{ref}}{\Delta T_{ref}}, & P_{cs} &= \frac{\rho c_s}{\rho c_{ref}}, & P_{cl} &= \frac{\rho c_l}{\rho c_{ref}}, & Ste &= \frac{\rho c_{ref} \Delta T_{ref}}{\rho L_f}, \\ P_k &= \frac{k}{k_{ref}}, & \tau &= \frac{a_{ref} t}{L_{ref}^2}, & z^* &= \frac{z}{L_{ref}}, & \varphi &= \frac{q L_{ref}}{\Delta T_{ref} k_{ref}} \end{aligned} \quad (2.31)$$

where $a_{ref} = k_{ref} / \rho c_{ref}$.

The introduction of those parameters in equations (2.4)-(2.10), leads to the dimensionless form of the one dimensional problem:

$$\frac{\partial \theta(z^*, \tau)}{\partial \tau} = \frac{P_k(z^*)}{P_{cs}(z^*)} \frac{\partial^2 \theta(z^*, \tau)}{\partial z^{*2}} + \psi(z^*, \tau; \theta) \quad \forall z^* \in (0, L^*), \forall \tau > 0 \quad (2.32)$$

with

$$\psi(z^*, \tau; \theta) = \frac{1}{P_{cs}} \frac{\partial \left[\left(\Delta P_c \left(\theta + \frac{T_{ref}}{\Delta T_{ref}} \right) + Ste^{-1} \right) f^*(\theta) \right]}{\partial \tau} \quad (2.33)$$

where $\Delta P_c = P_{cl} - P_{cs}$.

The liquid fraction is represented by:

$$f^*(\theta) = \frac{1}{2} \left[1 + \tanh \left(\frac{\theta}{\Delta \theta} \right) \right] \quad (2.34)$$

where $\Delta \theta$ is the dimensionless range of temperature where the phase change occurred.

The dimensionless form of the enthalpy-temperature function is given by:

$$H^*(\theta) = \frac{H(\theta)}{\Delta T_{ref} \rho c_{ref}} = \left[(1 - f^*(\theta)) P_{cs} + f^*(\theta) P_{cl} \right] \left(\theta + \frac{T_{ref}}{\Delta T_{ref}} \right) + Ste^{-1} f^*(\theta) \quad (2.35)$$

The continuity equation at the interface between the PCM and the insulated layer is written:

$$-P_{k,PCM} \frac{\partial \theta(z^*, \tau)}{\partial z^*} \Big|_{z^*=L_{PCM}^*} = -P_{k,IL} \frac{\partial \theta(z^*, \tau)}{\partial z^*} \Big|_{z^*=L_{PCM}^*} \quad \forall \tau > 0 \quad (2.36)$$

where $P_{k,PCM}$ and $P_{k,IL}$ represent the dimensionless thermal conductivities of the phase change material and of the insulated layer, respectively.

Then, the upper Dirichlet boundary condition is:

$$\theta(z^*, \tau) \Big|_{z^*=L^*} = \theta_\infty(\tau) \quad \forall \tau > 0 \quad (2.37)$$

where $\theta_\infty(\tau)$ represents the prescribed temperature. The lower side of the PCM is submitted to a prescribed heat flux as:

$$-P_{k,PCM} \frac{\partial \theta(z^*, \tau)}{\partial z^*} \Big|_{z^*=0} = \varphi(\tau) \quad \forall \tau > 0 \quad (2.38)$$

As for the initial condition, we assume: $\theta(z^*, \tau = 0) = \theta_\infty, \forall z^* \in (0, L^*)$.

The enthalpic form will be used in the following to simulate the exact dimensionless thermal fields:

$$\frac{\partial H^*(z^*, \tau)}{\partial \tau} = P_k(z^*) \frac{\partial^2 \theta(z^*, \tau)}{\partial z^{*2}} \quad \forall z^* \in (0, L^*), \forall \tau > 0 \quad (2.39)$$

Therefore, the measured thermal response θ_m is used for dimensionless temperature $\tilde{\theta}(z^*, \tau)$ and source terms fields $\tilde{\psi}(z^*, \tau; \theta)$ estimation. The corresponding dimensionless enthalpy-temperature function is calculated using:

$$\tilde{H}^*(\theta) = \tilde{P}_{cs} \left(\tilde{\theta}(\tau) + \int_{\tau=0}^{\tau_{end}} \tilde{\psi}(\tilde{\theta}) d\xi \right) \quad (2.40)$$

The quality of the estimated enthalpy-temperature function \tilde{H}_{PCM}^* is evaluated as:

$$rms = \sqrt{\frac{1}{n_\tau} \sum_{\tau=1}^{n_\tau} (\tilde{H}_{PCM}^*(\theta) - H^*(\theta))^2} \quad (2.41)$$

where H_{PCM}^* represents the exact dimensionless enthalpy-temperature function calculated using equations (2.34) and (2.35).

2.4.2 Numerical design

In this numerical study, the thermal response of the device for different sets of 4 dimensionless parameters ($P_{k,IL}$, $P_{c,IL}$, L_{IL}^* and φ) will be simulated using model (2.39) to obtain the measured dimensionless temperature θ_m .

The Table 1 summarizes the chosen reference parameters (see (2.31)):

Reference parameters	Value	
ρC_{ref}	$\rho C_{s,PCM}$	$J.m^{-3}.K^{-1}$
k_{ref}	k_{PCM}	$W.m^{-1}.K^{-1}$
L_{ref}	L_{PCM}	m
T_{ref}	T_f	$^{\circ}C$
ΔT_{ref}	1	$^{\circ}C$

Table 1: Reference parameters

Table 2 includes the values of studied sets of dimensionless parameters related to the device and the simulation.

Dimensionless parameter	PCM	Insulated layer	Simulation
P_k	1	$10^{-4}, 10^{-3}, 10^{-2}, 10^{-1}, 0.5, 1$	

P_c	$P_{cs} = 1, P_{cl} = 1.2$	$10^{-3}, 10^{-2}, 10^{-1}, 1, 10$	
L^*	1	0.5, 1, 2, 5, 10	
Ste^{-1}	50, 200		
T_f	0		
$\Delta\theta$	1		
φ_{\max}			0.2, 0.5, 1, 2, 5, 10
θ_{∞}			-20
$\theta(M, \tau = 0)$			-20
$d\tau$			0.05
Number of nodes	20	10	

Table 2: Dimensionless parameters for each layer and for the numerical simulations

It can be noticed that dimensionless parameters are chosen in order to cover a large range of possible scenarios, using a standard database of materials, about 250 from metals to insulated materials. With the choice of an insulated layer for the upper part of the device, all P_k ratios bigger than 1 are rejected as the corresponding P_c ratios. Thus, the studied parameters P_k and P_c (Table 2) cover more than 99% of the possible ratios between two thermal conductivities values or two specific heats values, respectively.

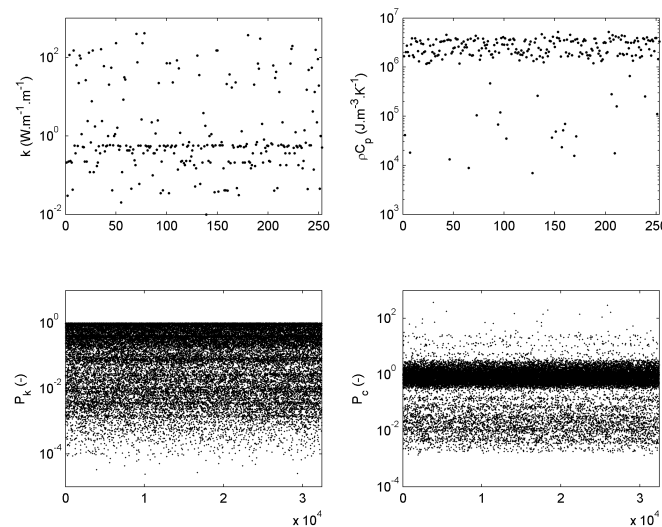


Figure 4: Thermal conductivity and specific heat for different materials and representations of all corresponding possible ratios

In a same way, the studied Stefan numbers cover a large range of scenarios (based on 126 different PCM) taking into account both values of latent heat and specific heat:

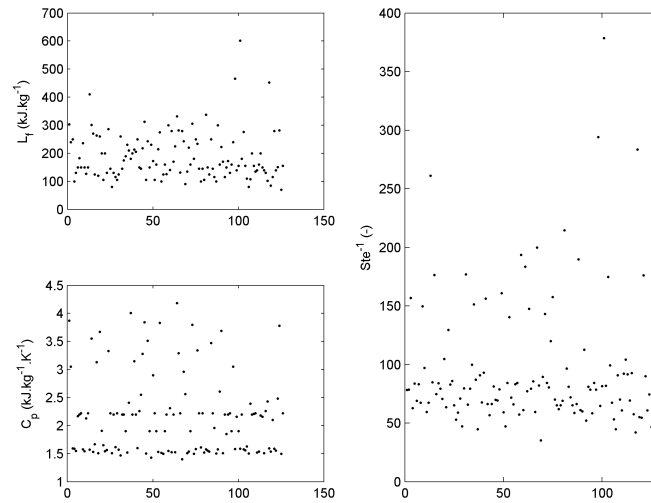


Figure 5: Latent heat and specific heat for different materials and representation of all corresponding possible ratios of Ste^{-1}

Finally, adding the tested dimensionless heat flux and thicknesses, a total of 1800 different scenarios were simulated.

2.4.3 Numerical results

To estimate a complete enthalpy-temperature function, the measured thermal response θ_m has to reach $\theta_{m3} = 20$ and $\theta_{m4} = -20$ during the period from τ_0 to τ_4 . Thus, if one of those temperatures is not achieved for a given configuration, the scenario is rejected. After simulation of the 1800 different scenarios, 694 of the tested configurations were rejected with this constraint. On the other hand, the quality of the estimated enthalpy-temperature functions is evaluated on the dimensionless temperature range $-15 \leq \theta \leq 15$. If the *rms* (Eq. (2.41)) is less than $Ste^{-1}/100$, the estimation is considered to be accurate. Figure 6 shows the less accurate kept results for each tested Stefan numbers:

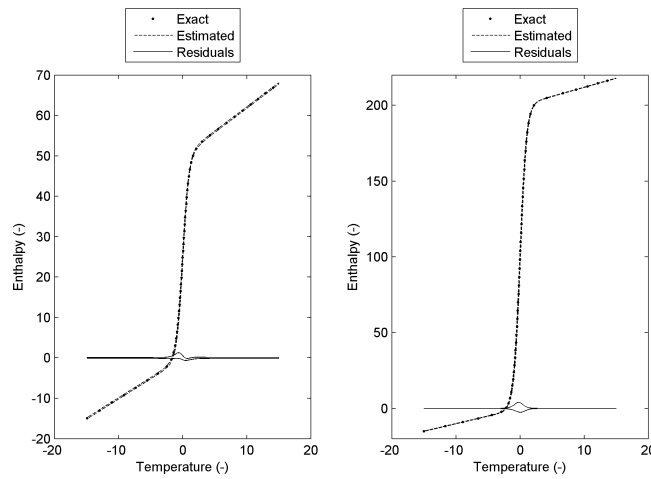
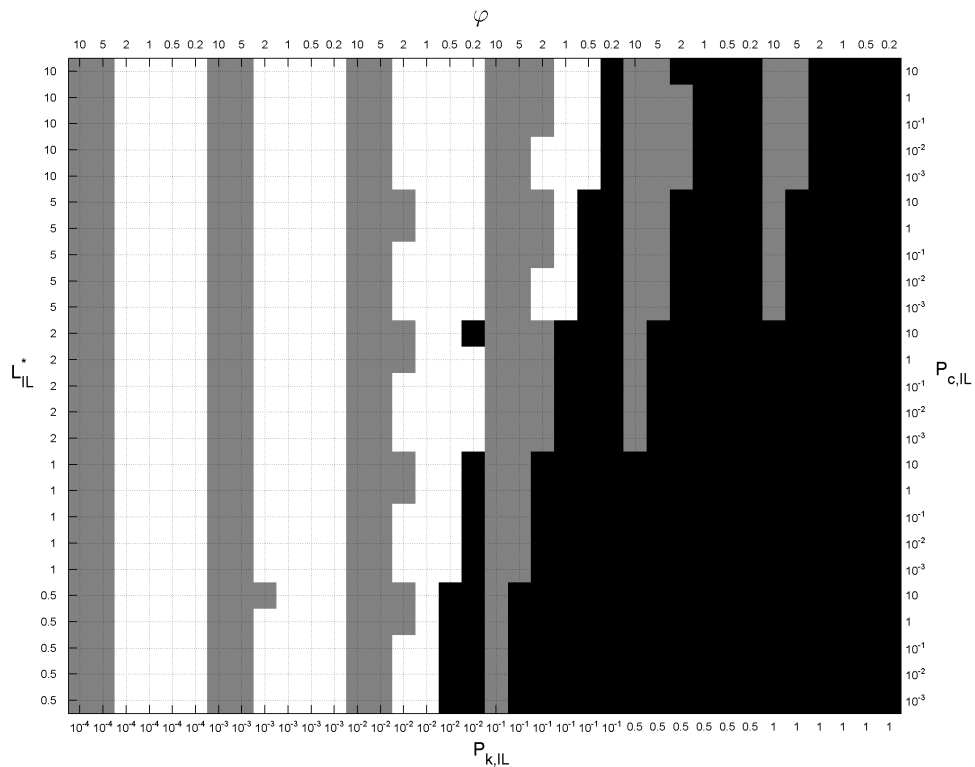


Figure 6: Less accurate enthalpy-temperature functions ($Ste^{-1} = 50, 200$ and $rms = 0.47, 1.99$, respectively)

In Figure 7, the results are shown for all the tested configurations ($Ste^{-1} = 50, 200$). The 694 rejected scenarios are represented in black. In the set of the 1106 other scenarios, the inaccurate results are in grey and the accurate ones are in white:



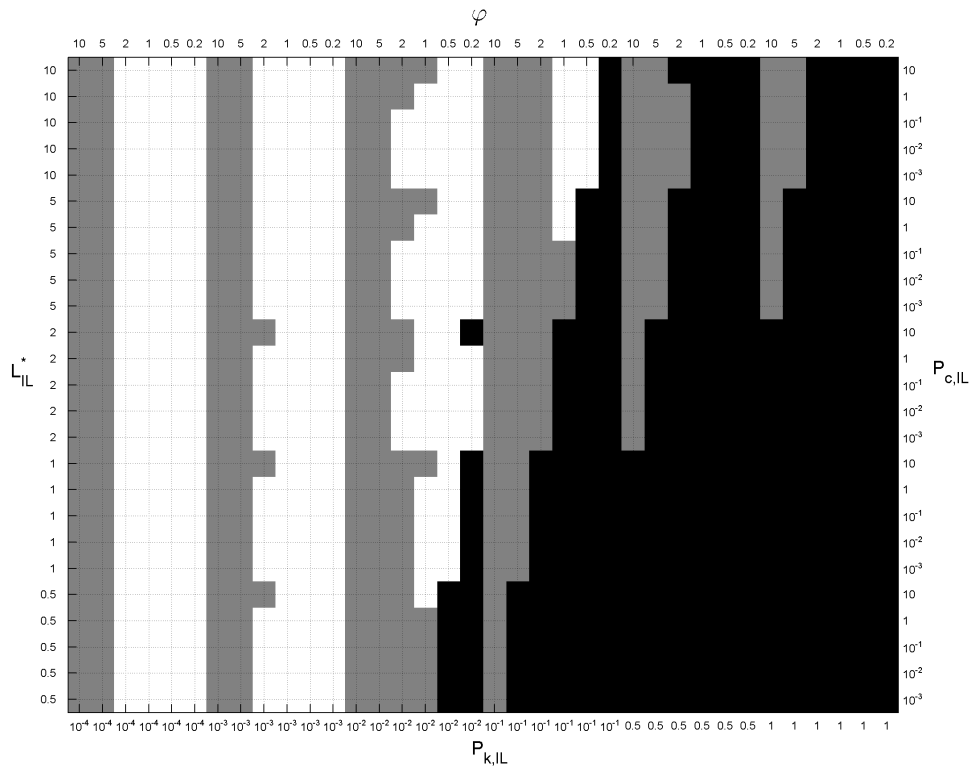


Figure 7: Results of the simulations and accuracy of the enthalpy-temperature functions estimations ($Ste^{-1} = 50,200$)

Some general remarks can be formulated studying those results. Obviously, the insulated layer has to be chosen to have the lowest as possible thermal properties with respect to the PCM ones. Ratios of 10^{-2} and 10^{-1} , or less, for thermal conductivities and specific heats, respectively, are a good choice when coupled with a ratio of thicknesses bigger than 1. Concerning the heat flux, the proposed inverse method is dependent on the thermal gradient in the PCM sample [17], i.e. the estimation of the enthalpy-temperature function is more accurate when this thermal gradient is low and therefore when the heat flux is low. Figure 8, depicting the *rms* as a function of different dimensionless heat flux or maximum thermal gradients between the two faces of the sample ($\max|\theta_{front} - \theta_m|$), illustrates this dependence:

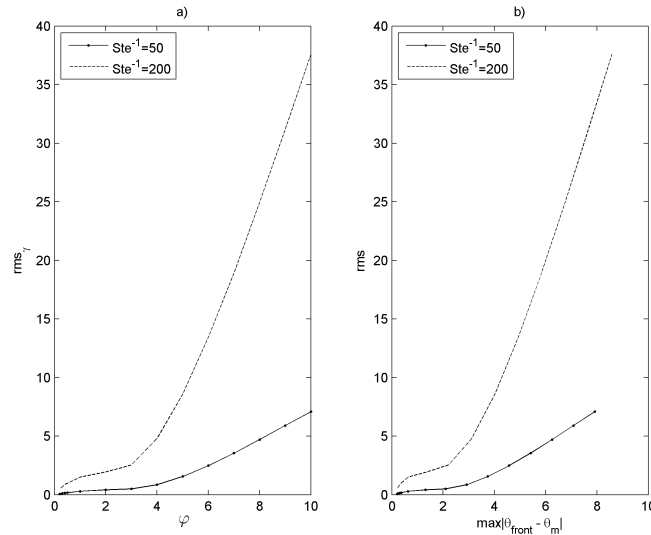


Figure 8: Accuracy of the inverse method with a) the dimensionless heat flux, and with b) the maximum of the thermal gradient within the sample ($P_{k,LL} = 10^{-2}$, $P_{c,LL} = 10^{-1}$ and $L_{LL}^* = 2$)

Experimentally, to overcome such a problem, a solution consists in controlling the temperature of the front face of the sample, adding a thermocouple between the heating element and the sample, to not exceed a given thermal gradient. Figure 10 represents a zoom on the *rms* obtained with the 1800 tested scenarios:

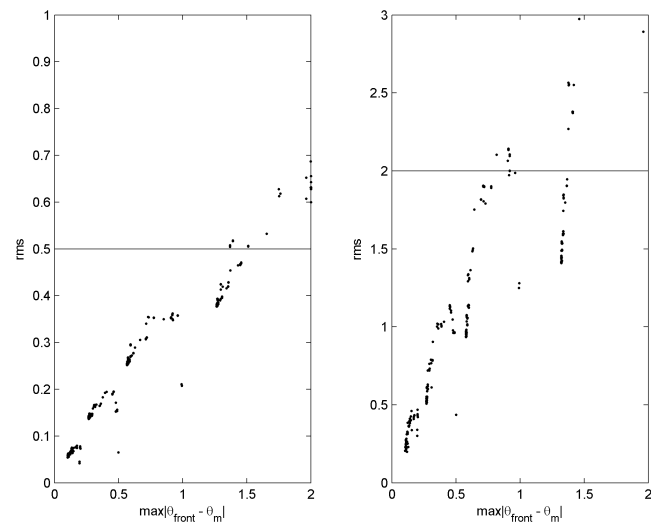


Figure 9: Zoom on the *rms* versus the corresponding maximum of thermal gradient within the sample with the limits of accuracy $Ste^{-1}/100$ ($Ste^{-1} = 50, 200$)

One observes that when the maximum of the thermal gradient doesn't exceed 1.5, the estimation of the enthalpy-temperature function is accurate. However, when the information on the thermal gradient is not available or when the obtained enthalpy-temperature function is not accurate, it is always possible to extract some relevant parameters from this estimation.

For example the less accurate result ($rms = 40.27$), shown in Figure 9, allows some basic estimations: the dimensionless specific heats in solid and liquid states through the slopes calculated before and after the melting point and the inverse of the Stefan number by evaluation of the gap between those two states. One notices that all those parameters can be obtain for both melting and cooling steps.

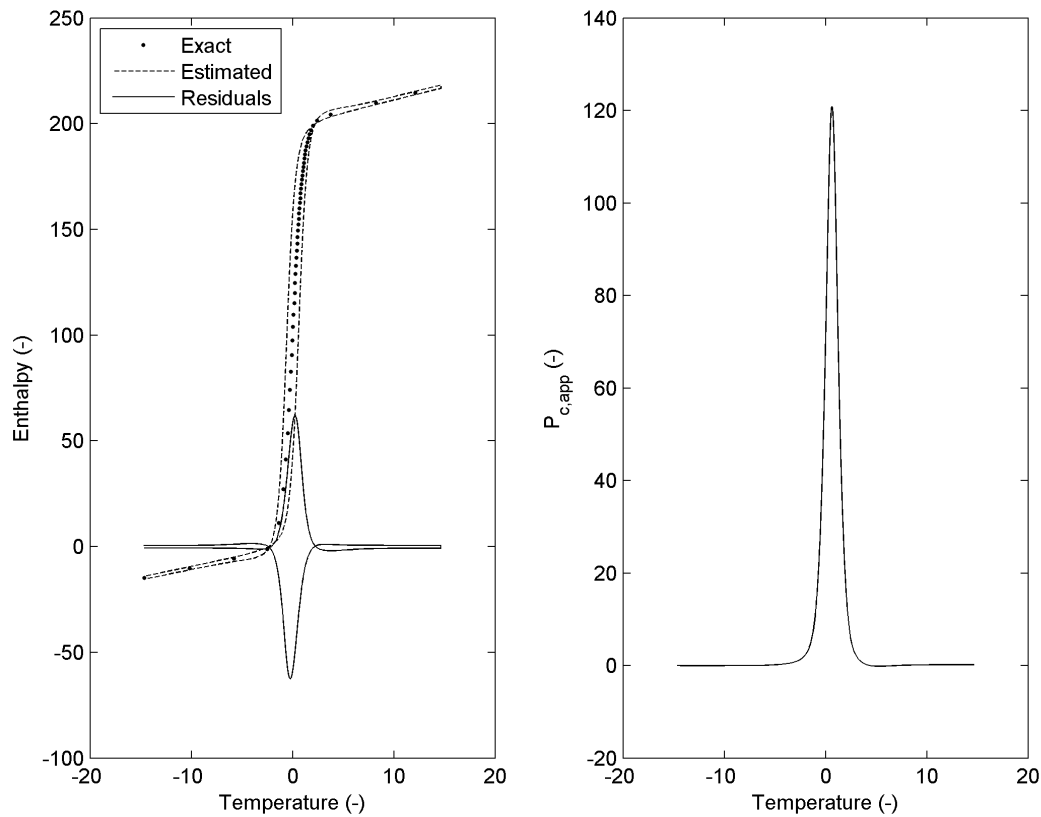


Figure 10: Less accurate enthalpy-temperature function and corresponding dimensionless specific heat

representation ($Ste^{-1} = 200$, $P_{k,IL} = 10^{-3}$, $P_{c,IL} = 10^{-3}$, $L_{IL}^* = 2$ and $\varphi = 10$)

In this example as in the following, the slopes giving the dimensionless specific heats in solid and liquid states estimations are calculated for the temperature range $-15 \leq \tilde{\theta} \leq -12$ and $12 \leq \tilde{\theta} \leq 15$, respectively. They are obtained by simple linear regressions. On the other hand, the inverse of the Stefan number is evaluated through an apparent specific heat representation, i.e. by integration of the peak obtained after derivation respect to the time of the enthalpy-temperature function (see Figure 10).

For the previous example, the estimated parameters are recapitulated in the Table 3:

Estimated parameter		Value	Error (%)
Melting	$P_{cs,PCM}$	1.004	0.4
	$P_{cl,PCM}$	1.197	0.3
	Ste^{-1}	200.27	0.13
Cooling	$P_{cs,PCM}$	0.995	0.5
	$P_{cl,PCM}$	1.2	0
	Ste^{-1}	200.3	0.15

Table 3: Estimated parameters ($Ste^{-1} = 200$, $P_{k,IL} = 10^{-3}$, $P_{c,IL} = 10^{-3}$, $L_{IL}^* = 2$ and $\varphi = 10$)

Finally, despite of a bad estimation of the enthalpy-temperature function, the thermodynamic parameters can be evaluated accurately. In summary, a device dedicated to the enthalpy-temperature function estimation has to be designed with some intuitive precautions, $P_{k,IL} \leq 10^{-2}$, $P_{c,IL} \leq 10^{-1}$, $L_{IL}^* \geq 1$ and $\varphi < 5$. Moreover, for a reasonable imposed dimensionless heat flux ($\varphi < 10$), if the phase changing occurs, i.e. if θ_m reaches $\theta_{m3} = 20$ and $\theta_{m4} = -20$, a good evaluation of the thermodynamic properties is always possible.

2.5 Experimental device and results

Considering the conclusions of the previous dimensionless numerical study, a device was designed to characterize a shape stabilized PCM. A Peltier element insure the heating-cooling of the sample and a heat flux sensor ($19.5 \mu V \cdot (W \cdot m^{-2})^{-1}$ of sensitivity) allows the control of this prescribed heat flux. Two type K thermocouples are used to record the thermal evolutions of the PCM and the ambient temperature. A good insulated layer with suitable mechanical properties is placed above a graphite foam filled with a PCM. The PCM has a melting point at about $40^\circ C$. A large piece of foam ($4cm \times 4cm \times 1.015cm$) is filled by imbibition with the PCM in liquid phase. The porosity of the foam (70%) is filled at 93% by the PCM. The data of the two layers are summarized in Table 4.

Parameters		
k_{IL}	0.023	$W \cdot m^{-1} \cdot K^{-1}$
ρc_{IL}	50000	$J \cdot m^{-3} \cdot K^{-1}$
L_{IL}	0.0255	m
$k_{G/PCM}$	100	$W \cdot m^{-1} \cdot K^{-1}$
$L_{G/PCM}$	0.01015	m
$\rho_{G/PCM}$	1010	$kg \cdot m^{-3}$
ρ_{PCM}	1046	$kg \cdot m^{-3}$

Table 4: Properties of the insulated layer and of the graphite/PCM composite

A cycle of melting – crystallization is performed in a range of temperature between 25 to 54°C in order to ensure a complete melting and crystallization of the PCM. Figure 11 presents the thermal response of the PCM (T_m) devoted to the enthalpy-temperature function estimation, and the prescribed boundary conditions in flux and temperature.

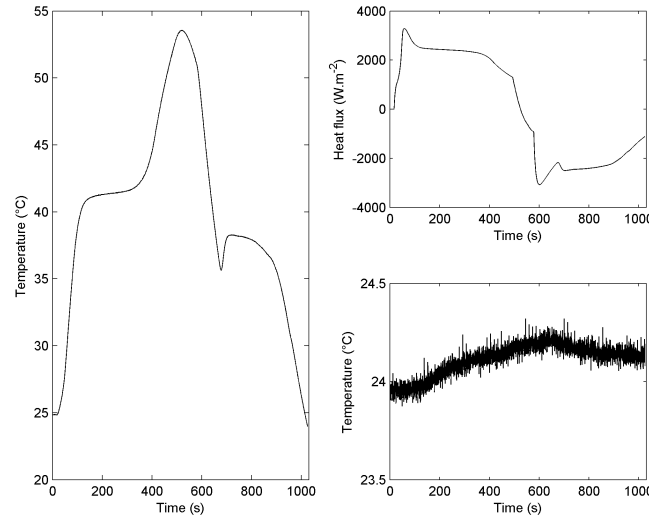


Figure 11: Thermal evolution $T_m(t)$ of the sample and boundary conditions ($q(t)$ and $T_\infty(t)$)

As this material presents an important undercooling, the estimation of the enthalpy-temperature function is done in the first part of the experimental protocol, i.e. during the heating of the sample, in accordance with the proposed inverse method. To initialize the calculus, the thermal conductivity of the composite is assumed equal to the graphite foam one and the specific heat in solid phase is arbitrarily 1×10^6 . The corresponding Tikhonov regularization parameter has been determined at $\mu = 0.05$.

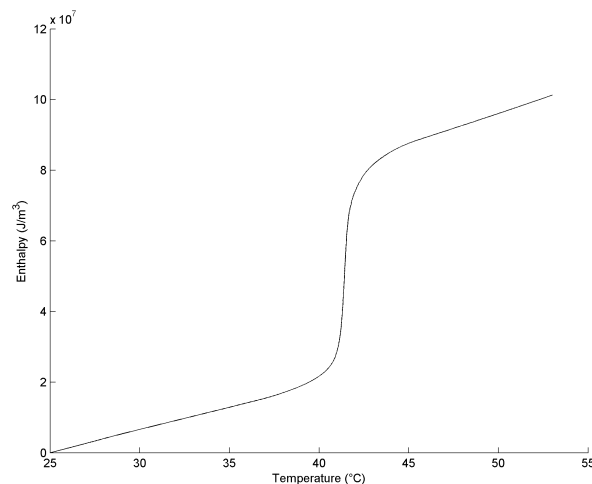


Figure 12: Estimated enthalpy-temperature function

The specific heats in solid and liquid states are calculated for the temperature ranges $25 \leq T_m \leq 30$ and $48 \leq T_m \leq 53$, respectively. As already pointed out, they are obtained by simple linear regressions. The latent heat ρL_f is evaluated by integration of the peak obtained in apparent specific heat representation of the enthalpy-temperature function ($d\tilde{H}/d\tilde{T}$, see Figure 13). It can be noticed that melting occurs, as expected, at about 40°C.

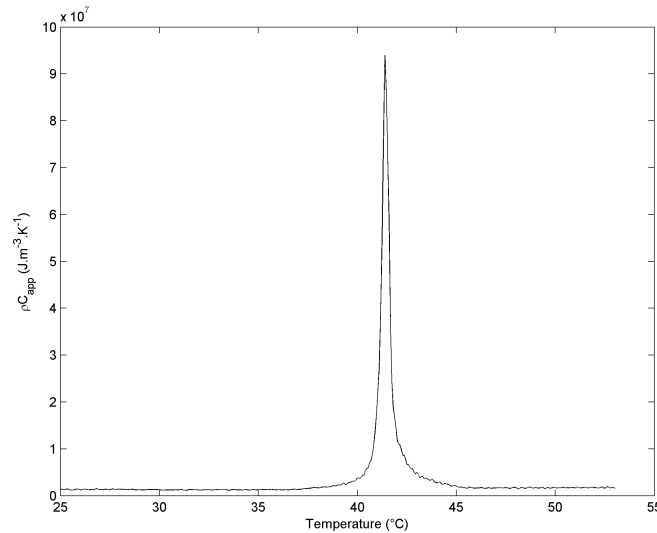


Figure 13: Apparent specific heat representation of the estimated enthalpy-temperature function

After the experiment, a piece of the tested sample was characterized using a standard DSC. The results obtained by the two methods are summarized in Table 5.

Parameters	DSC	Estimated	Error (%)	
$\rho c_{s,G/PCM}$	1.27×10^6	1.28×10^6	0.79	$J.m^{-3}.K^{-1}$
$\rho c_{l,G/PCM}$	1.63×10^6	1.7×10^6	4.3	$J.m^{-3}.K^{-1}$
ρL_f	5.02×10^7	5.15×10^7	2.6	$J.m^{-3}$

Table 5: Estimated thermodynamic properties of the graphite/PCM composite using a standard DSC and the proposed method

$\rho c_{s,G/PCM}$, $\rho c_{l,G/PCM}$ and ρL_f coming from the DSC have been calculated assuming no variation of density of the composite in solid and liquid phases. The results obtained by the proposed method are in very good agreement with the standard measurements. Two important skills of the method have to be considered. In a first time, due to the time integration (see eq. (2.7)), the estimated enthalpy-temperature function is not significantly affected by the measurement noise. The second skill is an “auto-correction” of a bad initialization of the specific heat in solid phase (here 1×10^6 instead of 1.27×10^6) through the estimation of the source term. Finally, one notices that enthalpy-temperature function estimation needs, in

this case, an experiment of less than 500 seconds, a testing time to compare with several days estimation with a standard DSC.

2.6 Conclusion

A new device for enthalpy-temperature function estimation of shape-stabilized PCM has been proposed. The simplicity of the experimental device is comparable to a hot plane one: a multilayer composed by a heating element, the studied PCM and an insulating layer. A heat transfer model has been used to obtain the enthalpy-temperature function from one temperature measurement point. A powerful inversion technique has been proposed for that. The main advantage of this technic is that it allows non-parametric identification of enthalpy-temperature functions. These functions are retrieved by solving a problem of time-dependent, moving sources estimation by inversion of a constant-parameters heat conduction model. It is shown that unknown sources are the output of a linear and invariant state model whose input is measured temperature on the upper side of the PCM. Enthalpy-temperature functions are thus calculated in a simple and fast way.

Using a dimensionless problem, many numerical tests carried out have shown the possibilities and limits of the proposed device. The main difficulty comes from the influence of the thermal gradient within the PCM, a large one forbidding accurate enthalpy-temperature function estimation but a simple thermodynamic characterization remain possible. The main advantages of the proposed method with regard to standard methods like DSC are that it yields complete thermodynamic characterization of PCM with large-size representative volumes in a testing time significantly reduced: some few minutes instead of several days as required for enthalpy-temperature function measurement when using DSC in isothermal step mode.

2.7 References

[1] S. Klarsfeld, F. De Ponte, F., Conductivité thermique des isolants, Techniques de l'ingénieur, Traité Mesure et Contrôle (2002) R2930.

[2] A. Degiovanni, Diffusivité et méthode flash, Revue Générale de Thermique 185 (1977) 420-441.

[3] B. Hay, J.R. Filtz, Batsale, J.C., Mesure de la diffusivité thermique par la méthode flash, Techniques de l'ingénieur (2004) R2955.

[4] T. Log, M.M. Metallinou, M.M., Thermal conductivity measurements using a short transient hot-strip method, Rev. Sci. Instrum. 63(8) (1992) 3966-3971.

[5] S.E. Gustafsson, Transient plane source techniques for thermal conductivity and thermal diffusivity measurements of solid materials, Rev. Sci. Instrum. 62(3) (1991) 797-804.

[6] X. Zhang, A. Dégiovanni, Mesure de l'effusivité thermique de matériaux solides et homogènes par une méthode de sonde plane, J. Phys. III 3 (1993) 1243-1265.

[7] X. Zhang, A. Dégiovanni, D. Maillet, D., Hot-wire measurement of thermal conductivity of solids: a new approach, High Temperatures, High Pressures 25 (1993) 577-584.

[8] M. Diot, M., Capacités thermiques, Techniques de l'ingénieur (1993) R 2970 – 1/12.

[9] C. Eyraud, A. Accary, A., Analyses thermique et calorimétrie différentielles, Techniques de l'ingénieur (1992) P1295_7.

- [10] M.J. Richardson, Quantitative aspects of differential scanning calorimetry, *Thermochimica Acta* 300 (1997) 15-28.
- [11] S. Rudtsch, S., Uncertainty of heat capacity measurements with differential scanning calorimeters, *Thermochimica Acta* 382 (2002) 17-25.
- [12] Y. Zhang, Y. Jiang, Y. Jiang, Y., A simple method, the T-history method, of determining the heat of fusion, specific heat and thermal conductivity of phase-change materials, *Meas. Sci. Technol.* 10 (1999) 201-205.
- [13] H. Hong, S.K. Kim, Y. Kim, Y., Accuracy improvement of T-history method for measuring heat of fusion of various materials, *Int. J. of Refrigeration* 27 (2004) 360-366.
- [14] A. Lázaro, E. Günther, H. Mehling, S. Hiebler, J.M. Marín, B. Zalba, Verification of a T-history installation to measure enthalpy versus temperature curves of phase change materials, *Meas. Sci. Technol.* 17, (2006) 2168-2174.
- [15] E. Günther, S. Hiebler, H. Mehling, Determination of the heat storage capacity of pcm and pcm-objects as a function of temperature, *Proc. 10th Int. Conference of Thermal Energy Storage, Ecstock 2006, New Jersey, 2006.*
- [16] J.-L. Dauvergne, E. Palomo Del Barrio, V. Morisson, A simple method for complete characterization of phase change materials, *J. Sol. Energy Eng. - November 2009 - Volume 131, Issue 4.*
- [17] J.L. Dauvergne, Réduction et inversion de modèles de diffusion thermique avec changement de phase, Ph.D. thesis, Université Bordeaux 1, Bordeaux, 2008.
- [18] V. Morisson, “Heat transfer modelling within graphite/salt composites: from the pore scale to the thermal energy storage system”, Ph.D. thesis, Université Bordeaux 1, Bordeaux, 2008.
- [19] Y. Jannot, Z. Acem, A. Kanmogne, Transient hot plate method with two temperature measurements for thermal characterization of metals (2006) *Measurement Science and Technology*, 17 (1), pp. 69-74.
- [20] P. Mounanga, G. Bastian, G. Bron, R. Coué, Rapid determination of the thermophysical properties of various materials. Method of the hot plane film, *Eur. Phys. J. Appl. Phys.* 26, 2004,p.65-72.
- [21] Z. Acem, Nouveaux composites graphite/sel destinés au stockage de l'énergie thermique à haute température : De l'élaboration au développement de méthodes de caractérisation thermique de matériaux conducteurs orthotropes, Ph.D. thesis, Université Bordeaux 1, Bordeaux, 2007.
- [22] J. Hadamard J., *Lecture on Cauchy's problem in linear partial differential equations*, Yale University Press, 1923.
- [23] J.V. Beck, B. Blackwell, C.R. St-Clair Jr, 1985, *Inverse Heat Conduction: Ill-Posed Problems*, Wiley Intersciences, New York, 1985.
- [24] O.M. Alifanov, *Inverse Heat Transfer Problems*, Springer-Verlag, Berlin Heidelberg, 1994.
- [25] N.H. Dinh, *Methods for Inverse Heat Conduction Problems*, Peter Lang, Frankfurt, 1998.

Advanced Spring School « Thermal Measurements & Inverse techniques », Domaine de Françon, Biarritz, March 1-6 2015

[26] D.A. Murio, The mollification method and the numerical solution of ill-posed problems, Wiley Intersciences, New York, 1993.

[27] A.N. Tikhonov, V.Y. Arsenin, Solutions of Ill-posed problems, V. H. Winston, Washington, DC, 1977.

[28] E. Palomo del Barrio, Multidimensional inverse heat conduction problems solution via Lagrange theory and model size reduction techniques, Inverse Problems in Science and Engineering 11(6) (2003) 515-539.

[29] A.E. Bryson, Y.C. Ho, Applied optimal control, Hemisphere, New York, 1975.

[30] P. C. Hansen, Analysis of Discrete Ill-Posed Problems by Means of the L-Curve, SIAM Review, Vol. 34, No. 4 (Dec., 1992), pp. 561-580.